Journal of Magnetism and Magnetic Materials 324 (2012) 3899–3905

Contents lists available at SciVerse ScienceDirect

Journal of Magnetism and Magnetic Materials

journal homepage: www.elsevier.com/locate/jmmm

Iron-based soft magnetic composites with Mn–Zn ferrite nanoparticles coating obtained by sol–gel method

Shen Wu [a], Aizhi Sun [a,*], Wenhuan Xu [a], Qian Zhang [a], Fuqiang Zhai [a], Philip Logan [b], Alex A. Volinsky [b]

[a] School of Materials Science and Engineering, University of Science and Technology Beijing, Beijing 100083, China
[b] Department of Mechanical Engineering, University of South Florida, Tampa, FL 33620, USA

ARTICLE INFO

Article history:
Received 27 February 2012
Available online 30 June 2012

Keywords:
Mn–Zn ferrite
Soft magnetic composite
Annealing treatment
Permeability

ABSTRACT

This paper focuses on iron-based soft magnetic composites which were synthesized by utilizing Mn–Zn ferrite nanoparticles to coat iron powder. The nanocrystalline iron powders, with an average particle diameter of 20 nm, were obtained via the sol–gel method. Scanning electron microscopy, energy dispersive X-ray spectroscopy and distribution maps show that the iron particle surface is covered with a thin layer of Mn–Zn ferrites. Mn–Zn ferrite uniformly coated the surface of the powder particles, resulting in a reduced imaginary permeability, increased electrical resistivity and a higher operating frequency of the synthesized magnets. Mn–Zn ferrite coated samples have higher permeability and lower magnetic loss when compared with the non-magnetic epoxy resin coated compacts. The real part of permeability increases by 33.5% when compared with the epoxy resin coated samples at 10 kHz. The effects of heat treatment temperature on crystalline phase formation and on the magnetic properties of the Mn–Zn ferrite were investigated via X-ray diffraction and a vibrating sample magnetometer. Ferrites decomposed to FeO and MnO after annealing above 400 °C in nitrogen; thus it is the optimum annealing temperature to attain the desired permeability.

1. Introduction

Soft magnetic composites (SMCs) are ferromagnetic particles coated with a thin electrically insulating layer and then pressed into the desired shape by the powder metallurgy (PM) methods. SMCs have unique magnetic properties, such as a three-dimensional (3D) isotropic ferromagnetic behavior, low eddy current loss, relatively lower total core loss at medium and high frequencies, and flexible design, which can be applied to various fields [1–5]. To provide the maximum magnetic permeability, the amount of inter-particle insulation should be minimized and the iron content maximized. Several researchers have tried to improve the magnetic performance of SMCs by selecting suitable insulating materials and applying various coating methods [6,7].

Currently, insulating coatings are commonly classified into two main categories: organic and inorganic coatings. Organic coatings are widely applied in SMCs due to their rapid and non-hazardous coating process and largely improved cured-film properties. These include epoxy, polyamide, silicone resins and polyvinyl alcohol [8–10]. The thermal treatment temperature for these materials is limited by the thermal resistance of the organic insulating layer between the magnetic particles; therefore phosphates (zinc/iron/manganese) and oxides (MgO) with high resistance temperatures were selected instead of organic coatings [11,12]. Unfortunately, the above mentioned insulating coatings have a common flaw. Being non-magnetic, the resulting SMCs have both decreased permeability and flux density. Therefore, developing novel SMCs with both a low loss and a high flux density has become a focus of modern SMC development.

In order to achieve this, Mn–Zn ferrites are chosen for their high electrical resistivity, suitable magnetic properties and high Curie temperature [13,14]. Mn–Zn ferrites are commonly produced by conventional ceramic processes, involving high temperature (1200 °C) solid-state reactions between the constituent oxides/carbonates. However, the method has some inherent drawbacks such as: (1) poor compositional control, (2) chemical inhomogeneity, (3) coarse particle size and (4) introduction of impurities during ball-milling/grinding [15]. In addition, the coarse and non-uniform particles, on compacting, result in the formation of voids or low-density areas in the green compacts. Wet chemical methods such as the sol–gel method [16] have overcome these drawbacks and produced homogeneous, fine and reproducible ferrite powders using aqueous solutions of salts of constituent ions.

In the present work, a new kind of SMC with Mn–Zn ferrite insulation, obtained by the sol–gel method, was produced and its magnetic properties measured and compared with epoxy resin coated powders. The effects of annealing on the structural and

* Corresponding author. Tel.: +86 10 823 76835; fax: +86 10 623 33375.
E-mail address: sunaizhi@126.com (A. Sun).

0304-8853/$ - see front matter © 2012 Elsevier B.V. All rights reserved.
http://dx.doi.org/10.1016/j.jmmm.2012.06.042

magnetic properties of the synthesized SMCs were also investigated.

2. Experimental details

2.1. Materials

The iron powder was supplied by Licheng Co., Ltd., with a particle size <150 μm. The purity of Fe was above 98%, containing $\sim$0.02 wt% C, 0.01 wt% Cu, 0.01 wt% Zn and some oxides. A widely used epoxy resin and hardener, supplied by Fluka, was used for comparison.

2.2. Preparation of Mn–Zn ferrite insulated powders via sol–gel method

The Mn–Zn ferrite powders ($Mn_{0.8}Zn_{0.2}Fe_2O_4$) were prepared, via the sol–gel method, using ferric nitrate ($Fe(NO_3)_3\cdot 9H_2O$), zinc nitrate ($Zn_2(NO_3)\cdot 6H_2O$), manganese nitrate ($Mn_2(NO_3)$), citric acid ($C_6H_8O_7\cdot H_2O$) and ammonia as raw materials. Equimolar metal nitrates and citric acid were dissolved in appropriate amounts of distilled water, and the solution pH value was adjusted to 6 with ammonia. The solution was heated to 60 °C and continuously stirred using mechanical agitation. After 3 h the solution became a homogenous viscous sol–gel. At this point, the sol–gel was oven dried at 120 °C for 12 h to obtain a dry gel. A loose, brown and very fine Mn–Zn ferrite powder was produced after the dried gel had spontaneously combusted in air. The iron powders were mixed with 3 wt% of obtained Mn–Zn ferrite powders (the iron powders to Mn–Zn ferrite powders mass ratio was 100:3) in a spiral mixer. The mixing procedure was carried out in acetone and stirred until the acetone evaporated.

2.3. Composite production

The epoxy resin and the Mn–Zn ferrite insulated powders were compressed into toroid samples (40 mm outer diameter, 32 mm inner diameter, and 4 mm height) at 500 MPa of pressure. The compaction of the samples was performed using zinc stearate as the die wall lubricant. Finally, the produced composites were annealed in nitrogen at 300, 400, 500 and 650 °C for 1 h. For comparison, green compacts (without annealing) were prepared from the epoxy resin. The Mn–Zn ferrite insulated powders and the uncoated powders were prepared and their magnetic properties were measured.

2.4. Characterization

The Mn–Zn ferrite insulating layer was characterized by scanning electron microscopy (SEM, ZEISS EVO 18, Germany) coupled with energy dispersive X-ray spectroscopy (EDS) and X-ray diffraction (Philips APD-10 diffractometer using Cu-Kα source). Coverage of the particles with a Mn–Zn ferrite coating was studied by elemental mapping to show the distribution of iron, oxygen, manganese and zinc. Hysteresis loops were measured using a vibrating sample magnetometer (VSM; LDJ 9600, LDJ Electronics, USA) with a maximum field of 10 kOe at room temperature. The complex permeability of the toroid samples was measured by an AC performance tester (NIM-3000, China, 400 Hz–500 kHz) at saturation flux density ($B_m=50$ mT). The electrical resistivity measurement was performed by using the four points probe method in accordance with the ASTM D4496-87 standard.

3. Results and discussion

3.1. Ferrites phase analysis and magnetic properties

Fig. 1 depicts the X-ray diffraction pattern of the auto-combustion powders. Comparing the XRD pattern of the synthesized particles with the standard diffraction spectrum (JCPDS: 10-0467), one can see that the synthesized powder has a pure spinel structure, which indicates that one can obtain a pure Mn–Zn ferrite phase via the sol–gel method. The average particle size was calculated to be 20.4 nm using Sherrer's equation [17]

$$L=K\lambda/\beta\cos\theta, \quad (1)$$

where L is equivalent to the particles' average core diameter, K is the grain shape factor ($K=0.94$); λ is the incident X-ray wavelength, β denotes the full width at half-maximum (in radians) of the highest intensity 311 powder diffraction reflection and θ is the corresponding diffraction angle ($2\theta=34.901^\circ$).

Hysteresis loops of as-received iron particles and synthesized Mn–Zn ferrite, under a 10 kOe magnetic field, are shown in Fig. 2. It is obvious that the magnetization of the as-received iron powders is much higher than that of the Mn–Zn ferrite. This behavior originates from the different magnetic properties of ferromagnetic and ferrimagnetic materials.

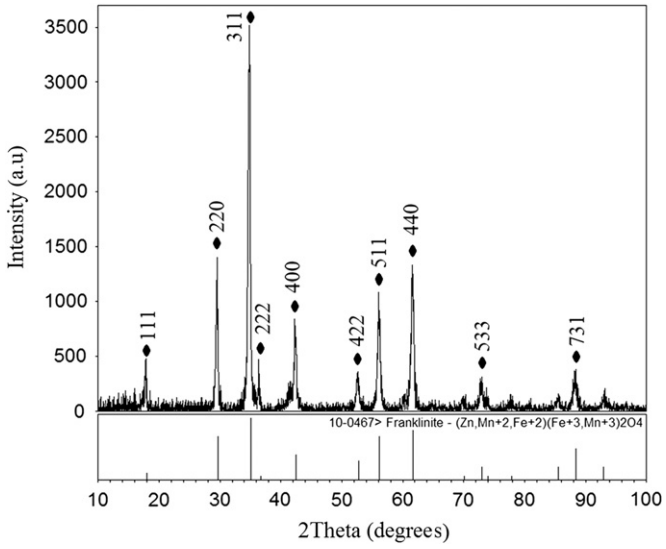

Fig. 1. XRD pattern of the auto-combustion powders.

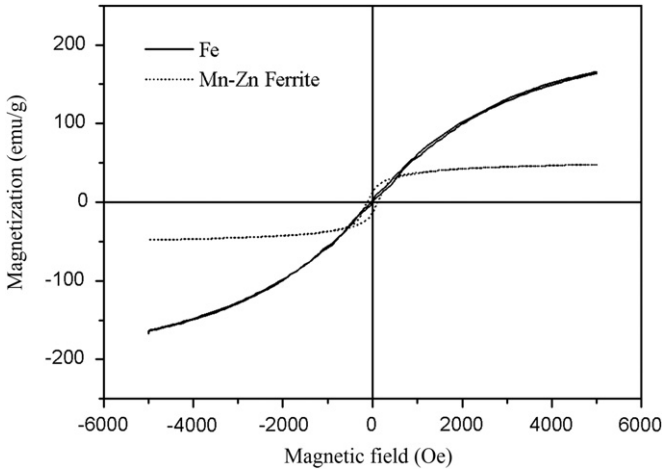

Fig. 2. Hysteresis loops of the Fe and Mn–Zn ferrite powders at 300 K.

3.2. Insulating layer characterization

For high-frequency applications, it is necessary to improve the electrical resistivity of the iron powder particles by adding a suitable electrically insulating material. An insulating material can create a thin layer on the iron powder particles and can separate metallic particles from one another. Fig. 3(a) and (b) shows SEM micrographs of pure iron and Mn–Zn ferrite coated iron powder particles, respectively. The fine white Ni–Zn ferrite powders on the coarse iron particles are seen in Fig. 3(b). Fig. 3(c) shows the EDX analysis of the Mn–Zn ferrite coated iron powders. The surface layer essentially consists of manganese, zinc, iron and oxygen; therefore, an iron–ferrite layer has been formed. With respect to the analyzed depth, the comparison among the intensities of the manganese, zinc and iron peaks seems to indicate that the Mn–Zn ferrite layer is thin.

The coverage of the iron powder surface by the iron–ferrite coating is indirectly shown by the maps of iron, manganese, zinc and oxygen distributions for the selected sample areas (Fig. 4). It can be concluded that each particle was coated by a uniform and thin Mn–Zn ferrite layer.

3.3. Insulating layer effect on magnetic properties

Fig. 5 shows the permeability of the uncoated samples and the green Mn–Zn ferrite insulated compacts at different frequencies. The change in the real part of the permeability of the Mn–Zn ferrite coated samples is almost negligible, which explains why the Mn–Zn ferrite coated samples have excellent frequency characteristics. At lower frequencies (<20 kHz), the real part of the permeability of the Mn–Zn ferrite coated samples is less than that of the uncoated samples. This can be explained by the presence of Mn–Zn ferrite layer—the magnetization of Mn–Zn ferrite is less than that of iron (Fig. 2), which results in a lower magnetic permeability. At higher frequencies (>20 kHz), the Mn–Zn ferrite coated powder, having a lower effective particle size, exhibits higher magnetic permeability as a result of the eddy current reduction. The smaller eddy current means a larger skin depth, which leads to a higher operating frequency and lower losses at high frequencies [18].

Fig. 6 shows the real part of the permeability versus frequency of the Mn–Zn ferrite and the epoxy resin insulated compacts. As seen in Fig. 6, the real part of the permeability of the samples coated in epoxy resin exhibits a lower value. At 10 kHz, the Mn–Zn ferrite insulated compacts ($\mu'=88.5$) exhibit better magnetic properties, with the real part of the permeability increasing by 33.5%, as compared with the epoxy resin coated samples ($\mu'=66.3$). The higher permeability for the Mn–Zn ferrite coated sample is attributed to its larger magnetic component, as the Mn–Zn ferrite layer is insulative, in contrast to the non-magnetic epoxy resin layer.

Fig. 7 depicts the variation of the magnetic loss for two different samples including Mn–Zn ferrite and the epoxy resin insulated particles at low and high frequencies. At low frequency, below 15 kHz, the Mn–Zn ferrite insulated compacts exhibit lower magnetic loss (Fig. 7(a)). The higher permeability means a lower demagnetizing field, which leads to lower hysteresis losses. The lower total loss was achieved from the Mn–Zn ferrite insulated compacts because of the small hysteresis loss. It was suggested that a Mn–Zn ferrite layer on an iron powder surface was effective in increasing permeability and restricting the magnetic loss. The Mn–Zn ferrite-coated samples show a low total magnetic loss, which is attributable to a higher flux density, when compared with conventional resin-coated samples.

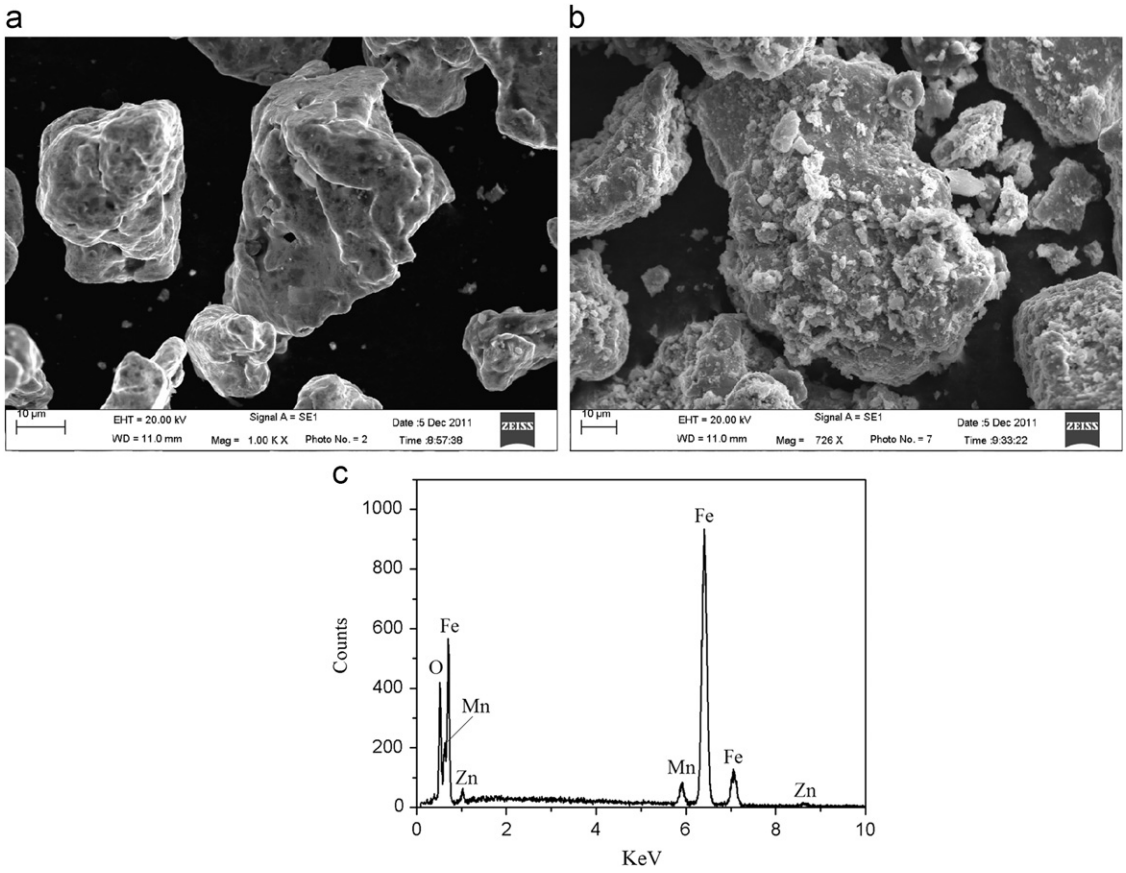

Fig. 3. (a) SEM image of pure iron powders; (b) SEM image of Mn–Zn ferrite insulated iron powders; and (c) EDS analysis of Mn–Zn ferrite insulated iron powders.

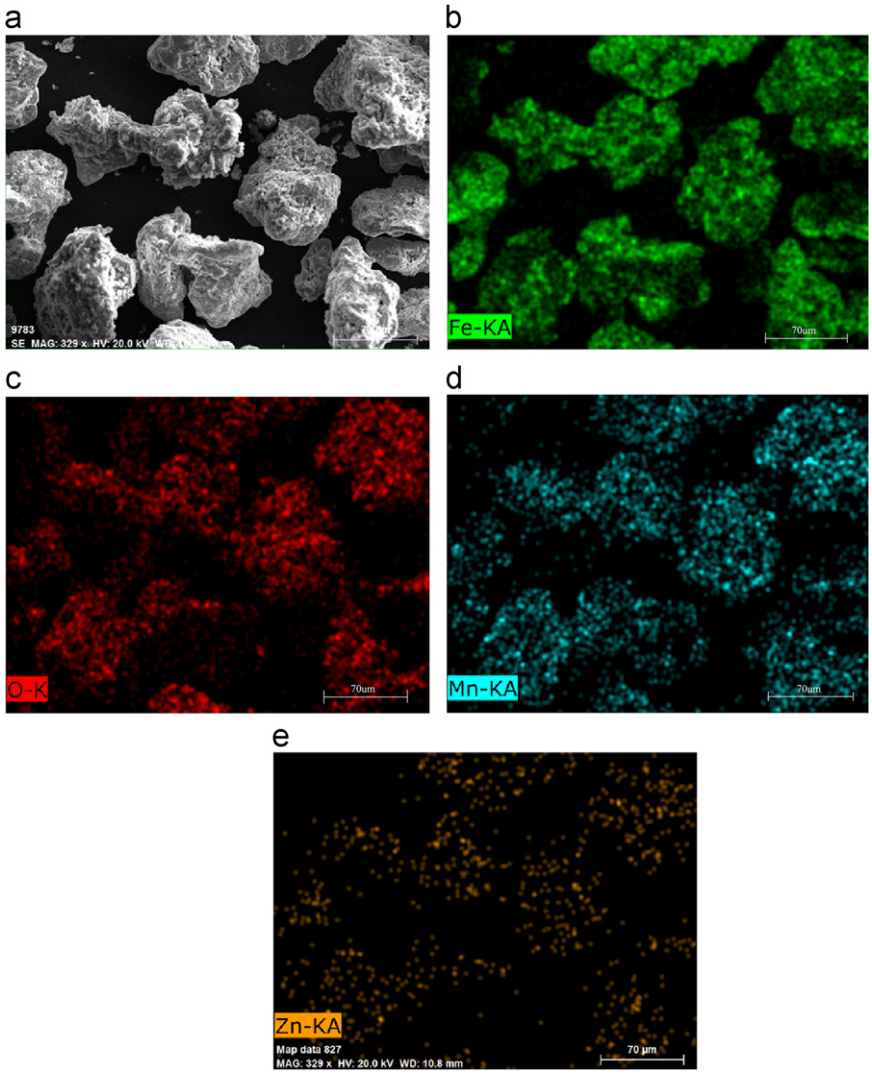

Fig. 4. Maps of oxygen, manganese, zinc and iron of Mn–Zn ferrite insulated iron powders.

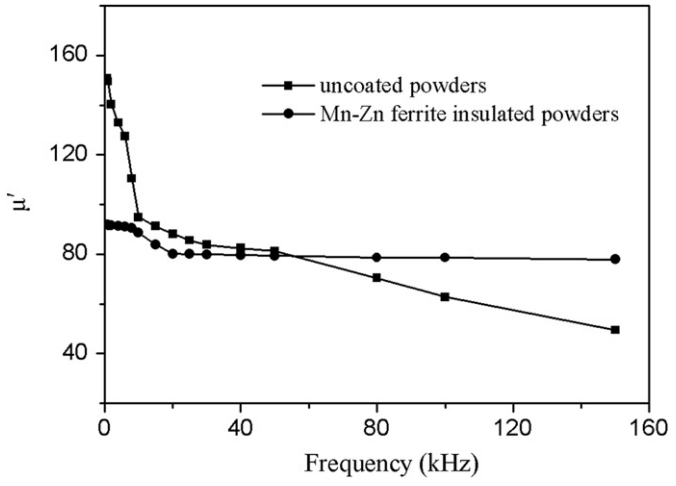

Fig. 5. Variation of real part of permeability for uncoated and green Mn–Zn ferrite insulated compacts with frequency.

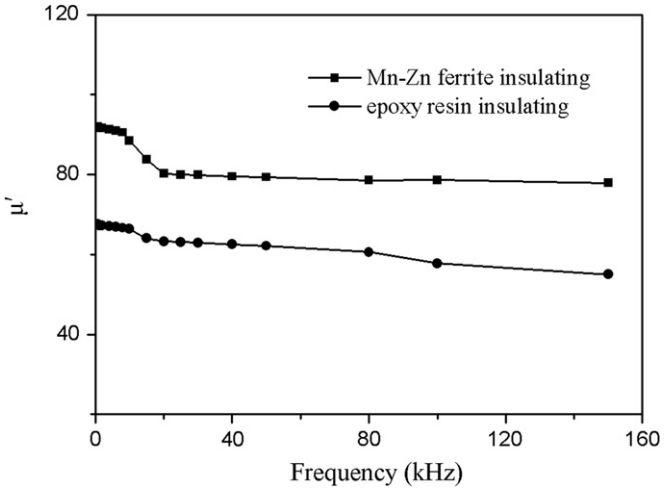

Fig. 6. Variation of real part of permeability with frequency for Mn–Zn ferrite and epoxy resin insulated compacts.

3.4. Annealing treatment effect on the magnetic properties

Fig. 8 shows the effect of the annealing temperature on the real part of the permeability of the Mn–Zn ferrite insulated compacts. The permeability of the annealed samples is higher than that of the green sample. The reason for this is that the compaction step always creates some plastic deformation in the

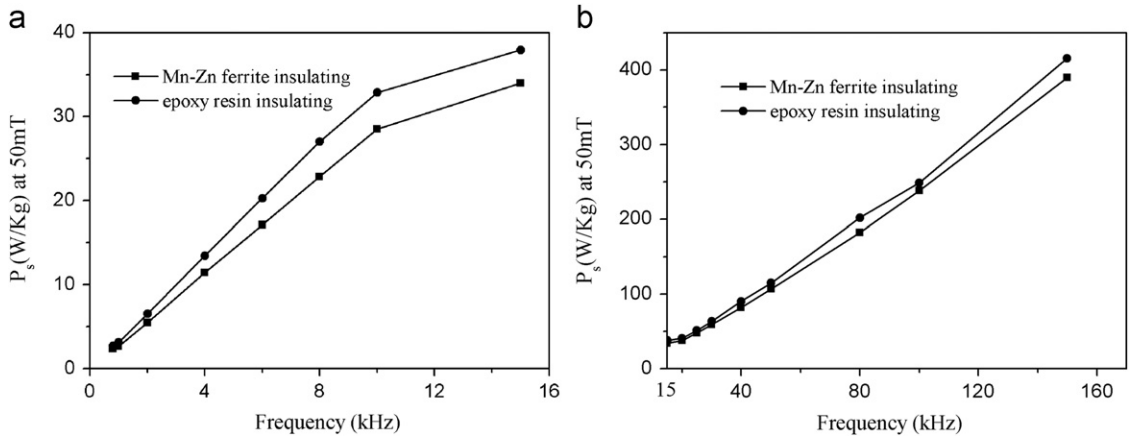

Fig. 7. Magnetic loss of the Mn–Zn ferrite and epoxy resin coated samples: (a) below 15 kHz and (b) above 15 kHz.

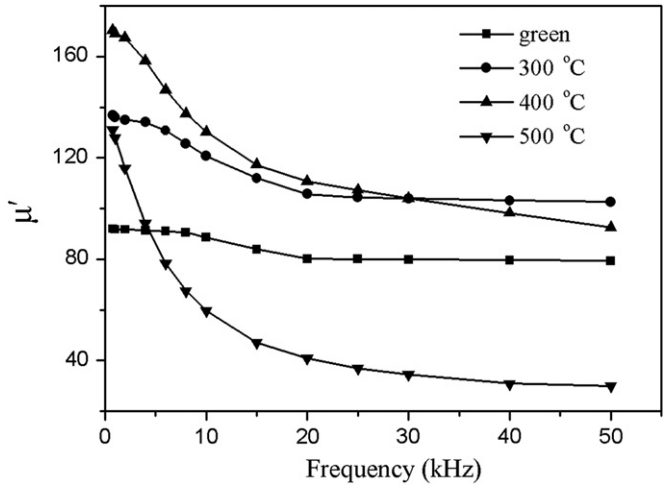

Fig. 8. Effect of annealing treatment at different temperatures on the real part of permeability of Mn–Zn ferrite insulated compacts.

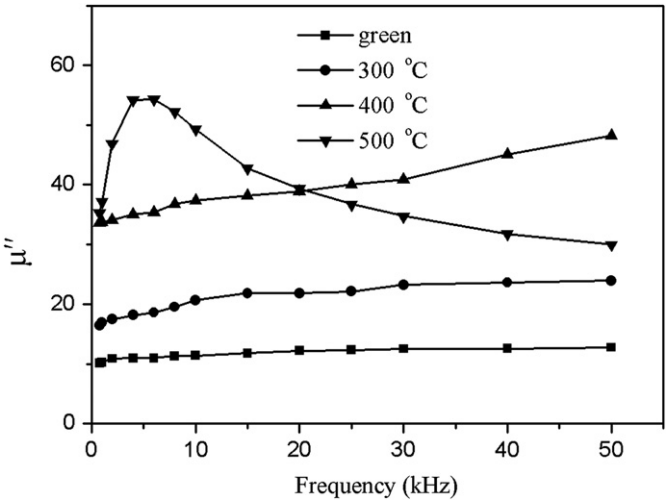

Fig. 9. Effect of annealing treatment at different temperatures on the imaginary part of permeability of Mn–Zn ferrite insulated compacts.

Table 1
Effect of annealing treatment on electrical resistivity of Mn–Zn ferrite coated compacts.

SMC	Without annealing	Annealed at 300 °C	Annealed at 400 °C	Annealed at 500 °C
Electrical resistivity ρ (μΩ m)	311.2	173.5	64.7	4.5

powder particles and consequently increases the dislocation density in the particles themselves. The dislocations act as pinning centers and impede the movement of the magnetic domain walls. The heat treatment permits low volume fraction of defects, reduces the distortion within the particles, lowers the dislocation density and thereby increases the magnetic permeability [19]. The real part of the permeability continuously decreases with frequency. The rate of this decline is faster at higher temperatures.

Table 1 shows the effects of the annealing treatment on the electrical resistivity of the Mn–Zn ferrite coated compacts. As a general trend, the electrical resistivity decreased with the annealing temperature. The resistivity of the composite material strongly depends on the amount of ferrite and the presence of defects, such as porosity, point defects, residual stresses, distortions and the dislocation density [18]. Annealing can reduce these imperfections and release the residual stress. Therefore, annealed compacts have a lower electrical resistivity.

Fig. 9 shows the variations of the imaginary part of the permeability for Mn–Zn ferrite insulated compacts, with respect to frequency, for different annealing temperatures. The annealing treatment increases the imaginary part of the permeability, especially for higher temperatures, as a consequence of the reduction in the electrical resistivity (Table 1). The imaginary part of the permeability is maximum when the samples are annealed at 500 °C. This peak value corresponds to the resonant frequency. The annealing treatment decreases both the anisotropy field and the electrical resistivity because of the stress reduction and also decreases the relaxation frequency (f_r) according to [20]

$$f_r = \frac{\rho}{2\pi\mu_0\mu_i d^2}. \quad (2)$$

Here, ρ is the specific electrical resistivity, μ_0 is the permeability of vacuum, μ_i is the initial permeability and d is the diameter of the particles. According to Fig. 8, annealing at 500 °C decreased f_r to about 5 kHz. As a result, the sample annealed at 500 °C exhibits a much lower electrical resistivity, a lower real permeability at high frequencies and a higher imaginary permeability. It has been confirmed that the insulating layer is failing at this annealing temperature.

Fig. 10 shows the XRD pattern of the Mn–Zn ferrite powders annealed at different temperatures for 1 h in a nitrogen atmosphere. The sample annealed in nitrogen at 400 °C has sharper and more intense XRD reflections, as compared to the non-annealing diffraction patterns, indicating good crystallinity. With an increase in the annealing temperature, the annealed powders contain some impurity XRD reflections, which are due to the FeO (JCPDS: 06-0615) phase. The annealed powders have FeO and MnO (JCPDS: 03-1145) phases. The Mn–Zn ferrite phase disappeared when annealing temperature reached 650 °C. This can be explained by the Mn and Fe elements having varying valencies within Mn–Zn ferrites. Therefore, oxidation and reduction reactions would probably occur in Mn–Zn ferrites. When the Mn–Zn ferrites are annealed in nitrogen, the oxygen partial pressure is lower than the ferrite decomposition pressure. Consequently, the decomposition reaction in ferrite occurs [21]:

$$MnFe_2O_4 \rightarrow FeO + MnO \quad (3)$$

The magnetic properties were measured by the VSM, at room temperature, for the auto-combusted ferrite powder and for the ferrite powders annealed at 400 °C and 650 °C in nitrogen, as shown in Fig. 11. It is clear that the 400 °C annealed ferrite powders have magnetic properties superior to the auto-combusted ferrite powder. On the contrary, the ferrite powder annealed at 600 °C has poor magnetic properties due to the formation of non-magnetic FeO and MnO phases.

From Table 1 and the above discussion, it is clear that the Mn–Zn ferrite layer fails above an annealing temperature of 400 °C. Meanwhile, the sample with the Mn–Zn ferrite insulation, annealed at 400 °C, has the highest real permeability and an acceptable imaginary permeability, when compared with the other annealed samples. As a result, it can be concluded that 400 °C is an optimal annealing temperature for Mn–Zn ferrite coated iron-based soft magnetic composites.

4. Conclusions

Iron-based soft magnetic composites with a Mn–Zn ferrite coating were synthesized and the effect of annealing treatments, of varying temperatures, on the magnetic properties was studied.

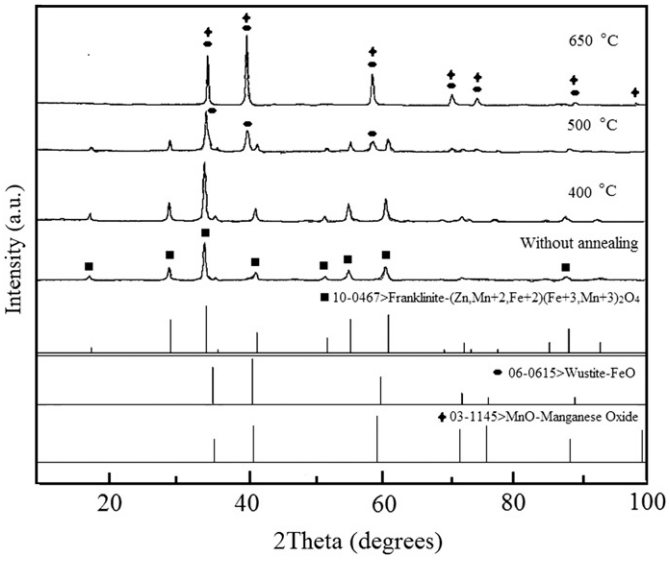

Fig. 10. XRD pattern of the Mn–Zn ferrite powders annealed at different temperatures.

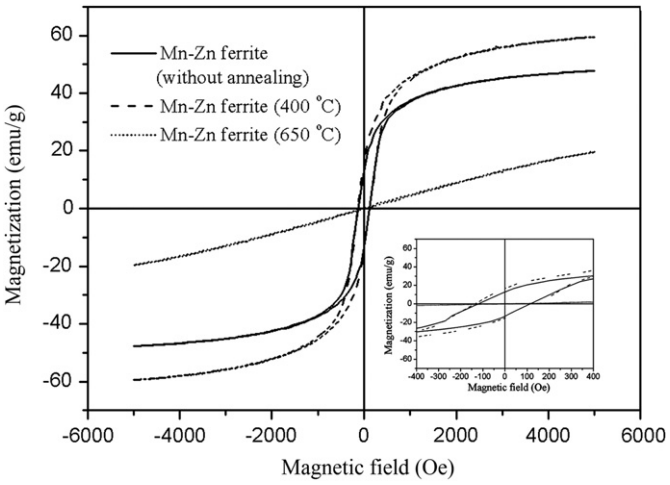

Fig. 11. Magnetic hysteresis loops of Mn–Zn ferrite powders annealed at different temperatures.

Conducted research may make it possible to develop low loss, high flux density, soft magnetic composites. The following conclusions could be drawn:

1. SEM, EDX analysis, and element distribution maps showed that the particle surface layer contains a thin insulating layer of Mn–Zn ferrite, with high particle surface coverage.
2. The Mn–Zn ferrite layer decreases imaginary permeability, as well as increases the electrical resistivity and the operating frequency.
3. The SMCs with a Mn–Zn ferrite coating had higher permeability and lower magnetic losses in a wide range of frequencies, in contrast to the conventional epoxy resin coated samples. For example, the real part of the permeability increased by 33.5%, when compared with the epoxy resin coated samples, at 10 kHz.
4. The sample with Mn–Zn ferrite insulation and annealed at 400 °C has the highest real permeability and an acceptable imaginary permeability, when compared with other annealed samples.

References

[1] E. Bayramli, O. Golgelioglu, H.B. Ertan, Journal of Materials Processing Technology 161 (2005) 83–88.
[2] S. Gimenez, T. Lauwagie, G. Roebben, W. Heylen, O. Van der Biest, Journal of Alloys and Compounds 419 (2006) 299–305.
[3] H. Shokrollahi, K. Janghorban, Journal of Materials Processing Technology 189 (2007) 1–12.
[4] Y. Yoshizawa, S. Oguma, K. Yamauchi, Journal of Applied Physics 64 (1988) 6044–6047.
[5] M. Anhalt, Journal of Magnetism and Magnetic Materials 320 (2008) 366–369.
[6] H.R. Hemmati, H. Madaah Hosseini, A. Kianvash, Journal of Magnetism and Magnetic Materials 305 (2006) 147–151.
[7] A.K.M. Akther Hossain, S.T. Mahmud, M. Seki, T. Kawai, H. Tabata, Journal of Magnetism and Magnetic Materials 312 (2007) 210–219.
[8] K.S. Narasimhan, M.L. Marucci, Magnetic Materials, in: Proceedings of the Conference, Euro PM (2003) 207–212, pp.
[9] A. Knop, W. Scheib, Chemistry and Application of Phenolic Resins, Springer, New York, 1979.
[10] Y. Zaks, J. Lo, D. Raucher, E.M. Pearce, Journal of Applied Polymer Science 27 (1982) 913–930.
[11] A.H. Taghvaei, H. Shokrollahi, K. Janghorban, Journal of Magnetism and Magnetic Materials 321 (2009) 3926–3932.
[12] A.H. Taghvaei, A. Ebrahimi, M. Ghaffari, K. Janghorban, Journal of Magnetism and Magnetic Materials 322 (2010) 808–813.
[13] S. Deka, P.A. Joy, Materials Chemistry and Physics 100 (2006) 98–101.
[14] P. Hu, H.B. Yang, D.A. Pan, H. Wang, J.J. Tian, S.G. Zhang, X.F. Wang, A.A. Volinsky, Journal of Alloys and Compounds 322 (2010) 173–177.

[15] J. Azadmanjiri, Journal of Non-Crystalline Solids 353 (2007) 4170–4173.
[16] A. Chatterjee, D. Das, S.K. Pradhon, D. Chakraverty, Journal of Magnetism and Magnetic Materials 127 (1993) 214–218.
[17] H.P. Klug, L.E. Alexander, X-ray Diffraction Procedures for Polycrystalline and Amorphous Materials, Wiley, New York, NY, 1997 637.
[18] H. Shokrollahi, K. Janghorban, Journal of Magnetism and Magnetic Materials 313 (2007) 182–186.
[19] K. Nishimura, Y. Kohara, Y. Kitamoto, M. Abe, Journal of Applied Physics 87 (2000) 7127.
[20] R. Barrue, F. Mazaleyrat, Handbook of Advanced Electronic and Photonic Materials and Devices, 2001.
[21] Z.G. Zhou, Ferrite Magnetic Materials, Science Press, Beijing, 1981 368–374.